IMPROVEMENTS IN THE COOLING CAPACITY AND THE COP OF A TRANSCRITICAL CO_2 REFRIGERATION PLANT OPERATING WITH A THERMOELECTRIC SUBCOOLING SYSTEM

D. Astrain[(a, b)*], A. Merino[(a)], L. Catalán[(a, b)], P. Aranguren[(a, b)], M. Araiz[(a, b)]
D. Sánchez[(c)], R. Cabello[(c)], R. Llopis[(c)]

(a) Engineering Department. Public University of Navarre, Campus de Arrosadia s/n, 31006 Pamplona, Spain.

(b) Smart Cities Institute, 31006 Pamplona, Spain

(c) Department of Mechanical Engineering and Construction, Jaume I University, Campus de Riu Sec s/n, 12071 Castellón, Spain.

*Correspondig author: david.astrain@unavarra.es
Phone: +34 948 169597, Fax: +34 948 169099

Abstract:

Restrictive environmental regulations are driving the use of CO_2 as working fluid in commercial vapour compression plants due to its ultra-low global warming potential (GWP_{100} = 1) and its natural condition. However, at high ambient temperatures transcritical operating conditions are commonly achieved causing low energy efficiencies in refrigeration facilities. To solve this issue, several improvements have been implemented, especially in large centralized plants where ejectors, parallel compressors or subcooler systems, among others, are frequently used. Despite their good results, these measures are not suitable for small-capacity systems due mainly to the cost and the complexity of the system.

Accordingly, this work presents a new subcooling system equipped with thermoelectric modules (TESC), which thanks to its simplicity, low cost and easy control, results very suitable for medium and small capacity plants. The developed methodology finds the gas-cooler pressure and the electric voltage supplied to the TESC system that maximizes the overall COP of the plant taking into account the ambient temperature, the number of thermoelectric modules used and the thermal resistance of the heat exchangers included in the TESC. The obtained results reveal that, with 20 thermoelectric modules, an improvement of 20% in terms of COP and of 25.6% regarding the cooling capacity can be obtained compared to the base cycle of CO_2 of a small cooling plant refrigerated by air. Compared to a cycle that uses an internal heat exchanger IHX, the improvements reach 12.2% and 19.5% respectively.

Key words: CO_2, subcooling, R744, thermoelectricity, transcritical, COP, computational model

Nomenclature

$\dot{Q}$	heat flow rate (W)
$\dot{W}$	electric power consumption (W)
$\dot{m}$	mass flow rate (kg/s)
A	area (m^2)
C	thermal capacity (J/ ºC)
COP	coefficient or performance
cp	specific heat (J/ kg ºC)
d	density (kg/m^3)
I	current (A)
k	thermal conductivity (W/ ºC m)
L	length (m)
M	number of thermoelectric modules
n	number
N	number of thermoelectric pairs
P	pressure (bar)
$\bar{q}$	volumetric heat generation rate (W/ m^3)
R^e	electric resistance (Ω)
R^t	thermal resistance (K/W)
T	temperature (ºC)
t	time (s)
V	voltage (V)
x	X axis
y	Y axis
z	Z axis

Greek symbols

Δ	Increment
α	Seebeck coefficient (V/K)
δ	derivative
η	efficiency
π	Peltier coefficient (V)
ρ	electrical resistivity (Ωm)
ρ^{sup}	superficial electrical resistivity (Ωm^2)
σ	Thomson coefficient (V/K)
v	specific volume (m^3/kg)

Subscripts

amb	ambient
cer	ceramic
che	cold heat exchanger
comp	compressor
cont	contact
co2	CO_2
dis	discharge
ev	evaporator
G	global
gc	gas-cooler
he	heat extender
hhe	hot heat exchanger
i	isentropic
IHX	internal heat exchanger
in	inlet
ins	insulation
Joule	Joule effect
m	mean
out	outlet
Peltier	Peltier effect
TEM	Thermoelectric module
TESC	Thermoelectric subcooler
tp	thermoelectric pair
scr	screws
Thomson	Thomson effect
u	union
V	volumetric

1. INTRODUCTION

Almost since their inception, vapour compression refrigeration systems have been subject to severe technological modifications due to strict regulations about the working fluids employed, not only in terms of safety aspects (toxicity and flammability), but also regarding environmental issues such as Global Warming and Ozone Depletion. In 1974 Rowland and Molina proved that CFC refrigerants have a huge impact on the Ozone Layer, high ODP values (*Ozone Depletion Potential*), leading to the signature of the Protocol of Montreal in 1987 that regulated their use. In Europe, the 2037/2000 Regulation [1] and the CE-1005/2009 Directive [2] appeared banning the CFCs refrigerants by 2000 and the HCFCs substances (that were the first alternative for the CFCs) by 2015.

Nowadays, new strict regulations are being developed because of the effect on Global Warming of certain gases employed in refrigeration. The limitation of the use is being made according to their Global Warming Potential (GWP). In this sense, the European Union has established the 2006/40/CE Directive [3] and the EU 517/2014 Regulation, known as "*F-Gas*", whose final version was released in April 16th of 2014 and entered into force in January the 1st of 2015 [4]. This regulation, more specifically the Article 11, prohibits the use of hermetically sealed refrigerators and freezers for commercial use that contain HFCs with GWP_{100} of 2500 or greater by January 1st 2020, and those containing HFCs with GWP_{100} of 150 or more by January 1st 2022.

Therefore, these rules are affecting not only future refrigeration systems but also the current ones because according to the Article 13, from 2020 on, only those systems with a charge size lower than 40 tons of CO_2 equivalent could be refilled with a working fluid with GWP_{100} of 2500 or more. Furthermore, the Spanish Government has imposed taxes for the refill of refrigerants with high GWP. As a consequence, those working fluids typically used in commercial refrigeration plants, such as R404A, R507A or even R134a, are tending to disappear in favour of the fourth generation of refrigerants with no ozone depletion potential and less GWP than the previous generations.

In this context, the use of CO_2 as refrigerant has taken a step forward owing to its high safety level (A1) and low global warming potential (GWP = 1). The plants that use this refrigerant work with high COPs in areas where the annual average temperature is below 15°C, improving even the performance of the baseline HFC systems [5]. However, when operating in warm climates, these systems need to work under transcritical conditions losing efficiency [6].

140 This issue is leading to an extended research of different systems that could increase the COP of the CO_2 plants
141 making them more competitive. Some researchers have proposed the use of CO_2 in two-stage plants both as
142 low temperature fluid in cascade systems [7], or in combination with a booster system that can reach higher
143 efficiencies when the ambient temperature is below 13°C according to some studies [8]. Another considered
144 option is ejector technology [9–11] to reduce exergy losses in the throttling processes, so that increments in
145 the COP up to 17 % can be achieved in single stage CO_2 plants [12] or higher when, in addition to the ejector,
146 an internal heat exchanger, IHX, is installed [13,14].
147 Parallel compressor or dedicated mechanical subcooling systems can also be employed to increase the
148 efficiency in transcritical CO_2 systems. Some theoretical studies show the advantages of both techniques
149 compared to different cascade cycles or booster configurations for warm climate areas [15]. Other research
150 studies have shown the importance of optimizing the temperature and capacity of the mechanical subcooling
151 system as well as the discharge pressure for different refrigerants [16]. Mechanical subcooling system consists
152 in using other vapour compression machine installed at the outlet of the gas-cooler, cooling down the
153 refrigerant in order to increase the specific cooling capacity. Experimental investigations prove the importance
154 of this configuration showing improvements in the whole system up to 30% in terms of COP and up to 56%
155 in terms of cooling capacity depending on the heat rejection temperature, the evaporation level and the
156 refrigerant used in the mechanical subcooling system [17,18].
157 However, all these steps have some drawbacks such as the increase in the cost of the plant and the added
158 difficulty to control the operation of the system under different conditions. Therefore, these technologies, that
159 are profitable for high capacity plants, are not suitable for small-capacity systems (around 200 W) such as
160 supermarket small-size cabinet refrigeration systems (beverage coolers, for example). As an alternative, this
161 work presents a new thermoelectric refrigeration subcooling system (TESC) devoted to producing a controlled
162 subcooling degree at the outlet of the gas-cooler in order to obtain similar advantages to those achieved with
163 the mechanical subcooling system.
164 Thermoelectric refrigeration uses Peltier effect to convert electricity into heat for cooling or heating [19]. This
165 refrigeration technique outperforms conventional vapour compression systems since thermoelectric devices
166 are more compact, more robust and silent, because they minimize the moving parts; allow a better control of
167 the temperature and do not require any working fluid. However, these systems need more electric power than
168 vapour compression ones [20,21]. This issue has restricted the scope of thermoelectric cooling to small

capacity applications such as refrigeration of electronic devices [22], [23], [24]or small domestic refrigerators, where the huge influence of the thermal resistances of the heat exchangers of the system is proven [25]. On this matter, relevant improvements have been achieved by the development of phase change heat exchangers [26–28], but the COPs are still much lower than the ones obtained with vapour compression cycles [29]. However there are novel thermoelectric applications such as the thermoelectric water dispenser unit which is able to supply cold and hot drinking water simultaneously [30] or the efficient thermoelectric distillation system developed for production of drinkable water [31]. On the other hand, significant improvements on thermoelectric cooling have been achieved studying variable leg cross-sectional areas introduced into two-stage thermoelectric coolers [32] or combining two-stage design with transient supercooling effect [33]. A great solution studied was the development of a hybrid refrigerator, combining both the thermoelectric and the vapour compression system [34–36] where better efficiency values were obtained thanks to the cascade configuration of the thermoelectric modules (TEM) and the vapour compression part.

The goal of this work is to achieve overall improvements in the efficiency and the cooling capacity of a transcritical CO_2 vapour compression system through the implementation of a thermoelectric subcooling system optimized for high COP values. For this purpose, a computational model, previously validated, has been developed to study the overall performance of the system and the influence of the main parameters as ambient temperature, heat rejection pressure, number of thermoelectric modules installed, voltage supplied to the modules and thermal resistance of the heat exchangers in the TESC.

2. DESCRIPTION OF THE PLANT AND THE STUDY CONDITIONS.

This section introduces the configuration of the refrigeration facility where the influence of the TESC will be computationally analysed. To that purpose a CO_2 transcritical refrigeration plant with a small cooling capacity of 170W and operating at an evaporation level of –10 °C with a constant useful superheating of 5K has been chosen. Figure 1 presents the three different configurations adopted to perform the analysis. The first configuration is the base cycle which includes a hermetic-reciprocating compressor, a gas-cooler, a double-stage expansion system including a back-pressure valve, a thermostatic valve and a liquid tank between both, and an evaporator. The second configuration includes to the base cycle an internal heat exchanger (IHX) [38] which is represented with dashed lines and has been previously modelled by Torrella *et al.* [39]. The third configuration adds to the base cycle a thermoelectric subcooler (TESC) installed at the inlet of the back-

197 pressure and modelled as will be detailed in the next Section.

198 The gas-cooler efficiency has been fixed to 95% according to experimental results previously presented by the
199 authors [37], while the compressor, a commercial hermetic reciprocating-compressor with a displacement of
200 0.5 cm^3 and a constant rotation speed of 2900 rpm, has been defined thought the expressions included in Table
201 1. The volumetric (η_V) and the global efficiency (η_G) have been adjusted from experimental data previously
202 published [18]. The polynomial adjustment of both efficiencies presented in Table 1 includes the range of the
203 independent variables used in the equation as well as the maximum deviation (e) and the standard deviation of
204 the adjustment (σ).

205 As it is shown in Figure 1, the thermoelectric subcooler is installed at the outlet of the gas-cooler, cooling
206 down the refrigerant from state 3 to 4. The TESC is formed by several Marlow DT12-8L thermoelectric
207 modules (TEMs) [40] whose cold face is in contact with a prism cold extender made of aluminium with
208 dimensions of 40 x 40 x 10 mm that transfers heat from the heat exchangers installed in the CO_2 line to the
209 ambient. The CO_2 heat exchangers are made up by a copper plate with dimensions of 160 x 60 x 10 mm with
210 6 mini channels of 6 mm of diameter through which the CO_2 flows. Each heat exchanger allows the allocation
211 of 4 TEMs with dimensions of 40 x 40 x 4 mm, as can be seen in Figure 1. Each DT12-8L TEM is compounded
212 by 127 Bi-Te thermocouples (p-type and n-type) with 1.4 x 1.4 x 1.3 mm of dimensions. The heat exchanger
213 of the hot side rejects the heat absorbed from the modules plus the electric power supplied to them. In this
214 case, two options have been referred to analyse the influence of the thermal resistances on the performance of
215 the TESC and the overall COP of the plant. Two options have been studied, water dissipation and air
216 dissipation. Regarding water dissipation, a heat exchanger with identical dimensions of the CO_2 heat exchanger
217 has been considered. With respect air dissipation, a phase change heat exchanger, a heat-pipe, has been
218 considered. In all cases, the bond interface between the TEMs and the heat exchangers is filled with a high-
219 thermal conductivity material in order to minimize the thermal resistance as was studied by [41] and the gap
220 not occupied by the modules is filled with an insulation material with a thermal conductivity of 0.09 W/m·K
221 and a thickness of 10 mm.

222 3. CALCULUS METHODOLOGY AND COMPUTATIONAL MODEL.

223 A computational model has been developed to study and optimize the performance conditions of the

transcritical CO_2 refrigeration system operating with the three configurations. The most challenging configuration to simulate is the base cycle with the TESC, being the other two configurations just simplifications of the entire computational model. This latter model is formed by two parts that interact one another: a CO_2 vapour compression model and a thermoelectric computational model. The CO_2 vapour compression model solves the thermodynamic cycle of the CO_2 transcritical vapour compression plant based on polynomial expressions adjusted from experimental data previously published [18]; the thermoelectric model solves the thermoelectric system that causes a subcooling before the back-pressure valve, between points 3 and 4 at the cycle represented in Figure 1. Hence, the entire cooling cycle is solved using the CO_2 computational model where the subcooling experimented between point 3 and 4 is obtained thanks to the thermoelectric model, as Figure 2 depicts.

This section firstly describes the CO_2 computational model. This model solves the simple vapor compression system, defined in the above section, with transcritical operation. Later, the thermoelectric model is described, and finally the calculation methodology is included.

3.1. CO2 computational model

This computational model solves the base cycle of the cooling system via Matlab. It is based on the resolution of energy balances at different elements of the cooling system. To that purpose, REFPROP is used to calculate the CO2 properties at the different interest points. The entry variables are: the evaporation temperature (T_o), the ambient temperature (T_{amb}) and the useful and non-useful superheats (USH and TSH). As the cooling system is working in transcritical operation, the pressure and temperature of the CO2 at the outlet of the compressor are independent variables, and thus at this type of installation the discharge pressure is an entry variable defined by the user [17,18], as it can be seen at the diagram of the calculation methodology of Figure 2. This pressure highly influences the operation of the installation, as it is presented through the Results and analysis discussion.

Using the entry variables the computational model calculates the evaporation pressure (P_o) and the temperatures of points 1 and 8, obtaining their enthalpy values.

$$T_8 = T_{ev,out} = T_o + USH \quad (1)$$

$$T_1 = T_{comp,in} = T_o + TSH \quad (2)$$

In order to show the thermodynamic state of point 2, the outlet of the compressor, the experimental expressions of the compressor obtained from a previously published work [18] and presented in Table 1 are used. Thanks to these expressions and the discharge pressure the enthalpy of point 1 is obtained.

Once the inlet and outlet points of the compressor are defined, using the volumetric efficiency of the compressor presented in Table 1, the mass flow of the refrigerant can be computed, as well as the consumption of the compressor.

$$\dot{m}_{co2} = \frac{\dot{V}_{comp}}{v_1 \cdot \eta_V} \tag{3}$$

$$\dot{W}_{comp} = \frac{\dot{m}_{co2}(h_{2s} - h_1)}{\eta_G} \tag{4}$$

Point 2, the outlet of the compressor or the inlet of the gas-cooler, is used to determine the rest of the points and the cooling power and COP of the system, thanks to the gas-cooler efficiency [39].

$$T_3 = T_{gc,out} = T_2 - \varepsilon_{gc}(T_2 - T_{amb}) \tag{5}$$

$$h_3 = f(T_3, P_{gc}) \qquad h_3 = h_4 = h_5 = h_6 \tag{6}$$

$$\dot{Q}_{o,base\ cycle} = \dot{m}_{CO2}.(h_8 - h_3) \tag{7}$$

$$COP_{base\ cycle} = \frac{\dot{Q}_{o,base\ cycle}}{\dot{W}_{comp}} \tag{8}$$

As the base cycle does not count with the TESC or the IHX, point 3 and 4 are similar. In case the IHX is included, equations (9)-(11) are used to compute the new values. If the base cycle including the TESC needs to be calculated the thermoelectric model is used as it is described in the following section.

$$\varepsilon_{IHX} = \frac{T_8 - T_1}{T_3 - T_8} \tag{9}$$

$$(h_1 - h_8) = (h_3 - h_4) \tag{10}$$

$$\dot{Q}_{o,with\ IHX} = \dot{m}_{CO2}.(h_8 - h_4) \tag{11}$$

3.2. Thermoelectric computational model

The TESC system is a thermoelectric refrigerator which consumes electric power to absorb heat from the CO_2 stream at the outlet of the gas-cooler emitting heat to the ambient. Hence, it is a cooling system mainly composed by TEMs and two heat exchangers, one on each side of the TEMs, respectively, as it was defined in Section 2 and shown in Figure 1.

The thermoelectric computational model has been designed from a previously published one developed for the design and optimization of a thermoelectric refrigerator [34,35], which was validated showing a maximum error of 8.3 %. This whole computational tool has been modified to solve the TESC system, including the typical thermoelectric equations that explain Seebeck, Peltier, Thomson and Joule effects, equations (12-15), and the heat transfer in transient state, equation (16). The properties of all the elements involved have been considered variable with temperature and the hypothesis taken into account are: isotropic materials, one-dimensional electric current and heat flow and same thermoelectric properties and geometry for the p-type and n-type legs of the thermoelectric modules.

$$\alpha_{\mathrm{AB}} = \frac{dE_t}{dT} = \alpha_A - \alpha_B \tag{12}$$

$$\dot{\mathrm{Q}}_{\mathrm{Peltier}} = \pm\pi_{\mathrm{AB}} I = \pm IT(\alpha_A - \alpha_B) \tag{13}$$

$$\dot{Q}_{Thomson} = -\sigma\vec{I}(\overrightarrow{\Delta T}) \tag{14}$$

$$\dot{Q}_{Joule} = R^e I^2 \tag{15}$$

$$d \cdot cp\frac{\delta T}{\delta t} = k\left(\frac{\delta^2 T}{\delta x^2} + \frac{\delta^2 T}{\delta y^2} + \frac{\delta^2 T}{\delta z^2}\right) + \bar{q} \tag{16}$$

The computational model is based on the implicit finite difference method. Hence, applying this method to Equation (16), Equation (17) is obtained.

$$\frac{1}{R^t_{a,1}}({T_1}' - {T_a}') + \cdots + \frac{1}{R^t_{a,N}}({T_N}' - {T_a}') + \dot{Q}_a = \frac{C_a}{\delta t}[{T_a}' - T_a] \tag{17}$$

Looking to equation (17) each node has a heat capacity assigned and it is connected to adjacent nodes by a thermal resistances. Hence, the TESC system to be simulated has been discretized as Figure 3 shows. Since the TEM is the most complex part of the entire system, each thermoelectric pair is discretized lengthways in 10 nodes and two extra nodes represent the ceramic plates. Besides another node represents the ambient, one

node the cold side heat extender and the cold extender, an extra node the hot side heat exchangers and the CO_2 stream is represented by the last two nodes. A total of 17 nodes are solved.The thermal resistances and the heat capacities can be estimated using Equations (18-20), with *i* being each of the nodes shown in Figure 3, M the number of modules and N the number of thermoelectric pairs.

$$R_{i,i+1}^{t} = \frac{L_{tp}/9}{MNk_{tp}A_{tp}} \quad i = 1, \dots, 9 \tag{18}$$

$$C_i = \frac{MNA_{tp}L_{tp}d_{tp}cp_{tp}}{9} \quad i = 2, \dots, 9 \tag{19}$$

$$C_i = \frac{A_{tp}L_{tp}d_{tp}cp_{tp}}{18} + \frac{A_uL_ud_ucp_u}{2} \quad i = 1,10 \tag{20}$$

Each of the thermoelectric nodes included into the thermoelectric pair present Joule and Thomson effects, while the end nodes (1 and 10) also need to include the heat flux due to Peltier and contact effects. Equation (23) is used to calculate the heat flux in the interior nodes whereas Equations (24-25) are used for the end ones.

$$\dot{Q}_i = MN\left(\rho_{tp,i}I^2\frac{L_{tp}/9}{A_{tp}} - \sigma_{pt,i}I\frac{T_{tp,i-1} - T_{tp,i+1}}{2}\right) \quad i = 2, \dots, 9 \tag{21}$$

$$\dot{Q}_1 = MN\left(\alpha_{tp,1}T_1I + \frac{\rho_u^{sup}}{A_{tp}}I^2 + \rho_{tp,1}I^2\frac{L_{tp}/18}{A_{tp}} - \sigma_{tp,1}I\left(T_1 - \frac{T_2 + T_1}{2}\right)\right) \tag{22}$$

$$\dot{Q}_{10} = MN\left(-\alpha_{tp,10}T_{10}I + \frac{\rho_u^{sup}}{A_{tp}}I^2 + \rho_{tp,10}I^2\frac{L_{tp}/18}{A_{tp}} - \sigma_{tp,10}I\left(\frac{T_9 + T_{10}}{2} - T_{10}\right)\right) \tag{23}$$

The ceramic plates of the thermoelectric modules, used as electric insulation, are grouped in one node for the hot side, and one node for the cold side, assuming that the entire plate is at the same temperature. The thermal resistances and heat capacities of these nodes are given by Equations (24-25), and the properties of the material are input parameters of the computational model.

$$R_{cer}^{t} = \frac{L_{cer}}{k_{cer}A_{cer}} \tag{24}$$

$$C_{cer} = A_{cer}L_{cer}d_{cer}cp_{cer} \tag{25}$$

Table 2 includes information about the different parameters of the DT12-8LTEMs used for the simulation [40]. The latter table presents the parameter name, their value, units and a short description of the parameters.

Finally, the electrical power supplied to the M TEMs is given by equations (26-29), where V_{supply} is an input of the model.

316 $$V = MN\left(V_{supply} - \left(\alpha_{tp,1}T_1 - \alpha_{tp,10}T_{10}\right) + \sigma_{tp,1}\left(T_1 - \frac{T_2 + T_1}{2}\right) + \sigma_{tp,10}\left(\frac{T_{10} + T_9}{2} - T_{10}\right)\right.$$

317 $$\left. + \sum_{i=2}^{9}\left(\sigma_{tp,i}\frac{T_{i-1} - T_{i+10}}{2}\right)\right) \quad (26)$$

318 $$R_{TEM}^{e} = N\left(\rho_{tp,1}\cdot\frac{L/18}{A_{tp}} + \rho_{tp,10}\cdot\frac{L/18}{A_{tp}} + \sum_{i=2}^{9}\left(\rho_{tp,i}\cdot\frac{L/9}{A_{tp}}\right) + \frac{2\cdot\rho_{u}^{sup}}{A_{tp}}\right) \quad (27)$$

319 $$I = \frac{V}{R_{TEM}^{e}} \quad (28)$$

320 $$\dot{W}_{TESC} = MV_{supply}I \quad (29)$$

321 The cooling process of the CO_2 inside the TESC is modelled by two nodes. The first one represents the fluid
322 at the inlet of the subcooler, where $T_{TESC,in}$ is the temperature at the gas-cooler outlet (the temperature of point
323 3 in Figure 1). This is an entry parameter to the thermoelectric computational model which is obtained obtained
324 from the CO_2 model. The thermal resistances of the heat exchanger between the CO_2 and the TEM have been
325 calculated referring to the mean temperature of the fluid inside the subcooler. Thus, the second node represents
326 this mean point, and its temperature $T_{TESC,m}$ will be estimated by the model itself. The thermal resistance that
327 connects both nodes, R_{co2}^{t}, is given by equation (30,) and the heat capacity of the CO_2 will be estimated for
328 each temperature and pressure.

329 $$R_{co2}^{t} = \frac{\left(T_{TESC,in} - T_{TESC,m}\right)}{\dot{Q}_{o,TESC}} = \frac{1}{2\dot{m}_{co2}cp_{co2}} \quad (30)$$

330 Where

331 $$\dot{Q}_{o,TESC} = \dot{m}_{co2}cp_{co2}\left(T_{TESC,in} - T_{TESC,out}\right) \quad (31)$$

332 $$T_{TESC,m} = \frac{T_{TESC,in} + T_{TESC,out}}{2} \quad (32)$$

333 The thermal resistances for the hot side and the cold side heat exchangers, R_{che}^{t} and R_{hhe}^{t}, are given by the
334 design of each heat exchanger used in the system and they would be parameters of the study. Nonetheless, the
335 heat extender placed between the TEMs and the cold side heat exchanger is the same in all cases. Its thermal
336 resistance and heat capacity are obtained by Equations (33-34), where thermal contact resistance is also taken
337 into account using some experimental values from previous work [41].

338 $$R_{he}^{t} = \frac{L_{he}}{Mk_{he}A_{he}} + R_{cont}^{t} \quad (33)$$

$$C_{he} = MA_{he}L_{he}d_{he}cp_{he} \quad (34)$$

$$R^t_{cont} = 18.75\frac{A_{TEM}}{M} \quad (35)$$

To simulate the heat transferred directly from the hot to the cold heat exchangers through the insulation material bypassing the thermoelectric modules, another thermal resistance is included and estimated using Equations (36-38).

$$R^t_{thermal\ bridge} = \frac{R_{scr}R_{ins}}{R_{scr} + R_{ins}} \quad (36)$$

$$R^t_{ins} = \frac{L_{ins}}{k_{ins}A_{ins}} = \frac{L_{TEM} + L_{he}}{k_{ins}(A_{che} - MA_{he})} \quad (37)$$

$$R^t_{scr} = \frac{L_{scr}N}{A_{scr}k_{scr}n_{scr}} \quad (38)$$

The equation system obtained is non-linear, since the heat fluxes due to the thermoelectric effects are function of the temperature and the thermoelectric properties of the materials and the CO_2 also vary with this parameter. To solve this system, an iterative process is made, which calculates the temperatures for instant *t*, updates the thermal resistances and heat flux rates, and, finally, calculates the temperatures for instant *t+1*. Once the iterative process has finished, the temperatures of all nodes can be calculated, and thus the outlet temperature of the TESC is obtained and introduced into the CO_2 computational model, as Figure 2 shows.

3.3. Calculus methodology

To solve the CO_2 refrigeration system including the TESC both computational models need to interact. The CO_2 computational model starts solving the different points of the system (Figure 1) thanks to the energy balances included in the previous section and once it arrives to the outlet of the gas-cooler, the temperature at this point is introduced into the thermoelectric computational model. The latter model solves the thermoelectric phenomena using the outlet temperature of the gas-cooler and provides the outlet temperature of the TESC, T_4 at Figure 1. The CO_2 computational model using the temperature of point 4 closes the cycle and computes all the operating parameters. The cooling capacity of the base cycle and its COP can be obtained using equations (8)-(9). Moreover, the cooling capacity and COP of the TESC, the cooling capacity and COP of the base cycle including the TESC and the cooling capacity of the base cycle including the IHX can be computed.

$$\dot{Q}_{o,TESC} = \dot{m}_{CO2}.(h_4 - h_3) \quad (39)$$

$$COP_{TESC} = \frac{\dot{Q}_{o,TESC}}{\dot{W}_{TESC}} \quad (40)$$

$$\dot{Q}_{o,with\,TESC} = \dot{m}_{CO2}.(h_8 - h_4) \quad (41)$$

$$COP_{with\,TESC} = \frac{\dot{Q}_{o,base\,cycle} + \dot{Q}_{o,TESC}}{\dot{W}_{comp} + \dot{W}_{TESC}} \quad (42)$$

$$\dot{Q}_{o,with\,IHX} = \dot{m}_{CO2}.(h_8 - h_4) \quad (43)$$

As the cooling cycle has transcritical operation, the discharge pressure needs to be varied with the aim of finding the pressure that maximizes the COP of the installation [17, 18, 39]. Moreover, the voltage supplied to the TESC needs to be varied, as the subcooling changes as the voltage does and consequently the operation of the entire cooling cycle. Hence, the optimum voltage supply needs to be found for each discharge pressure. Both variables have been marked in red in Figure 2 to show the calculus methodology that seeks the optimum operation of the system.

In order to look for the optimum working point of the system, each discharge pressure studies different voltage supplies. Specifically, the ranges studied for the discharge pressure and the voltage supply are from 74 to 120 bars with increments of 0.5 bar and from 0.5 to 4 V in steps of 0.5 V respectively. In this way, since the gas-cooler pressure and the voltage supplied to the TEMs are related, the optimum values for these parameters can be achieved in an iterative process.

Besides, along the Results and discussion section other variables have been changed in order to see their influence on the operation of the system. The number of TEMs (M) and the thermal resistances of the heat exchangers located on both sides of the TEMs (R^t_{hhe} and R^t_{che}) have been modified to see their effect on the outputs of the model. These variables have also been highlighted in red in Figure 2.

The following parameters have been defined in order to represent the relative increment of cooling power due to the TESC system:

$$\Delta\dot{Q}_o = \frac{\dot{Q}_{o,with\,TESC} - \dot{Q}_{o,base\,cycle}}{\dot{Q}_{o,base\,cycle}} \quad (44)$$

$$\Delta\dot{Q}_{o\,IHX} = \frac{\dot{Q}_{o,with\,TESC} - \dot{Q}_{o,with\,IHX}}{\dot{Q}_{o,with\,IHX}} \quad (45)$$

388 This calculus methodology is adopted in the next section to explore the influence of the thermal resistances
389 of the hot and cold side heat exchangers in the TESC system. Similarly, this calculation process will be adopted
390 to determine the effect of installing several number of TEMs modules in the facility.

391

392 ## 4. RESULTS AND DISCUSSION

393 Following the methodology explained in section 3, this part is devoted to analysing the influence of the main
394 TESC parameters on the overall performance of the refrigeration facility. Thus, the effect of the gas-cooler
395 pressure, the operating voltage of the TEMs, the use of different number of modules, and the thermal
396 resistances for the heat exchangers, have been considered in order to determine the sensitivity of the TESC
397 system. To perform this analysis, three different ambient temperatures have been taken into account with the
398 aim to cover a wide range of heat rejection temperatures: 25, 30 and 35 °C.

399 ### 4.1. Influence of the gas-cooler pressure and the voltage of the TEMs

400 To assess the influence of the heat rejection pressure and the operating voltage of the TEMs, the number of
401 modules has been fixed to four and the thermal resistances for the hot and the cold side of thermoelectric
402 modules have been set to 0.06 K/W and 0.3 K/W, respectively.

403 Figure 4 shows the overall COP of the facility dependent on the gas-cooler pressure for the base cycle, the
404 system including the IHX, and the cycle including the TESC for different voltages supplied to the
405 thermoelectric modules. For the two ambient temperatures plotted, it can be noted that the use of an IHX
406 always improves the COP of the base cycle. This improvement depends on the ambient temperature as the
407 higher the temperature, the better the improvement. Nevertheless, the adoption of a TESC system performs
408 better improvements than the IHX most of the time. In this case, the improvement depends on the operating
409 voltage of the TEMs modules. Thus, for 35ºC, whatever the voltage selected, the improvement of the TESC is
410 higher, but operating at 30ºC, the improvement is lower than the IHX if the voltage is set to 4 V.

411 On the other hand, it is evident the existence of an optimum pressure that maximizes the COP of the system
412 for each ambient temperature, which is reduced when the IHX or the TESC system is added. This fact allows
413 the plant to operate with lower pressures, therefore reducing the compression ratio and improving the
414 efficiency of the compressor.

To check the effect of the voltage supplied to the TEMs on the refrigeration system, Figure 5 represents the maximum COP of the analysed configurations as a function of the voltage supplied. Additionally, in the same Figure, the COP of the TESC has been included.

According to the results depicted in Figure 5, as the voltage supplied to the modules increases, two opposite effects occur. On the one hand, an increment on the voltage leads to an increase in the cooling capacity of the modules, achieving a higher subcooling degree that benefits the specific cooling capacity of the facility and allows a reduction in the optimal heat rejection pressure. On the other hand, the increment of the voltage causes a drop in the efficiency of the TEMs since they work with a higher temperature difference between their faces, increasing the electrical power consumption of the plant. Consequently, as it can be seen in Figure 5, there is an optimum voltage that maximizes the overall COP, which is higher with greater ambient temperatures. This means that it exists a voltage that produces a subcooling which takes precedence over the efficiency loss of the TEMs. Regarding the cycle cooling capacity, as expected, there is a constant increase as the voltage supplied to the modules grows.

Finally, Table 3 summarizes the results obtained for the optimum values of the gas-cooler pressure and the optimum voltage supplied to the 4 TEMs considered, for each ambient temperature. In all the cases, the use of the TESC is beneficial, since it increases up to a 10.4 % the overall COP in relation to the base cycle and up to 3.5 % compared to the cycle with an IHX. The cooling capacity is also increased, achieving an improvement of 16.9 % in relation to the base cycle and of 11.2 % compared with the system that includes the IHX. It is necessary to remark that this cooling capacity may be far increased when supplying higher voltages to the modules, which can be very useful to face transient stages or during the star-up process.

As expected, the higher the ambient temperature, the lower the values of COP or cooling capacities obtained. However, the improvements reached with the TESC system are more significant as the ambient temperature increases. This is beneficial because it is under those conditions when the improvements of the system are more important.

4.2. Influence of the number of TEM

The methodology employed in the previous analysis has been repeated in order to study the influence of the number of TEMs installed on the refrigeration system. For each number of thermoelectric modules considered,

442 the gas-cooler pressure and the electric voltage supplied to the TESC system have been varied.

443 Figure 6 shows the overall COP of the system for different gas-cooler pressures and number of thermoelectric
444 modules installed on the TESC system, considering a fixed ambient temperature of 35°C, a fixed supply
445 voltage of the modules of 2 V and a fixed evaporation temperature of -10 ºC. From Figure 6 it can be noted
446 that with more thermoelectric modules installed, the degree of subcooling achieved is higher, causing an
447 increase in the specific cooling capacity and, consequently, an increase in the cooling capacity and in the COP
448 of the system. Moreover, more TEMs allow a reduction in the gas-cooler pressure that maximizes the COP of
449 the system, minimizing the compression ratio of the refrigeration facility.

450 Values from Figure 6 can be improved by varying the supply voltages of the TEMs, since their COP is strongly
451 influenced by this value. The results of this study are shown in Figure 7, where the optimum COP (according
452 to the gas-cooler pressure) is represented with respect to the voltage supply for different number of TEMs. As
453 it can be seen, the higher the number of modules installed, the higher the increments of the cooling capacity.
454 This parameter also grows as the operating voltage increases, while the COP of the TEMs rapidly decreases
455 with increasing voltages. Accordingly, for each number of installed TEMs, there is a voltage value that
456 optimizes the overall COP of the whole system. It is remarkable to note that the optimum voltage is lower as
457 the number of TEMs increases, and that the maximum COP achieved corresponds to the maximum number of
458 modules represented in the Figure 7 in this case.
459 Considering the combination of gas-cooler pressure and voltage supplied to the TEMs that optimize the COP,
460 Figure 8 shows the variation of this overall COP with respect to the number of thermoelectric modules included
461 in the TESC system, for an ambient temperature of 35°C. An increase in the number of modules improves the
462 COP, but the slope decreases progressively reaching a constant value of 1.46. In this way, the selection of the
463 number of modules that should be included in a TESC system must be done considering both energetic and
464 economic requirements, since a higher number of modules would increase the cost of the installation (more
465 devices would be needed), as well as the size of the exchanger, which would be bigger.

466

467 **4.3. Influence of the thermal resistances**

468 In thermoelectric systems, both for electric generation or for cooling, the heat exchangers employed at both

sides of the thermoelectric modules play a crucial role in their efficiency [42]. Hence, if the thermal resistance on the hot side decreases, the hot face temperature of the TEM will be closer to the ambient temperature. Something similar happens on the cold side, where low thermal resistances will bring the temperature of the cold face of the TEM closer to the CO_2 temperature. In this way, the lower the thermal resistances at both sides, the lower the temperature difference between faces of the TEMs. In this subsection, these parameters have been explored to study their influence on the efficiency of the TEM and on the overall COP of the plant.

Considering an ambient temperature of 35 °C; a TESC system with 4 thermoelectric modules installed, each of them supplied with a voltage of 2 V; and a gas-cooler pressure of 90 bar. Figure 9 shows the effect of the thermal resistance of the heat exchangers on the TEMs. As the value of these variables increases, there is an increment on the temperature difference between the faces of the modules, which leads to lower COP values of the TESC system.

Since a variation in the thermal resistances causes a variation in the optimum values for the supplied voltage and the gas-cooler pressure, it is necessary to perform the resolution methodology considering these new values.

A computational analysis using ANSYS-Fluent CFD software has been carried out to define the study interval of thermal resistances for the cold side heat exchanger, between the CO_2 flow and the cold face of the TEMs. The geometry analysed is a 180 mm x 60 mm copper plate, 10 mm thick, with 6 longitudinal channels with diameter 6 mm through which the CO_2 flows. This plate allows to install 4 thermoelectric modules. When 8, 12 or 16 TEMs are considered, it would be necessary to install 2, 3 or 4 heat exchangers in series. The mass flow considered in this study is 3.6 kg/h and the results show a variation of the thermal resistances between 0.35 and 0.7 K/W. Therefore, the interval employed for the analysis is the following:

$$R_{che}^{t} = (0.3 \quad 0.4 \quad 0.5 \quad 0.6 \quad 0.7 \quad 0.9) \ [K/W]$$

To set the range of the thermal resistances of the hot side, the values considered have been taken from a previous work about thermoelectric refrigeration [42] that covers a wide range of heat exchangers: finned dissipaters, water cooling systems and phase change heat exchangers, such as heat-pipes. Hence, the interval for the study is the following:

$$R_{hhe}^{t} = (0.03 \quad 0.06 \quad 0.09 \quad 0.12 \quad 0.15 \quad 0.20) \ [K/W]$$

Figure 10 shows the overall COP for the plant with respect to the voltage supplied to the TEMs, obtained for the optimum gas-cooler pressure. Each curve represents the COP for a certain combination of the best and worst thermal resistance values considered in this study, this is, $R^t_{hhe} = 0.03\ K/W$ and $R^t_{che} = 0.3\ K/W$; and $R^t_{hhe} = 0.2\ K/W$ and $R^t_{che} = 0.9\ K/W$; respectively for 4, 12 and 20 thermoelectric modules installed. With high thermal resistances (empty-boxes curves) the COPs achieved are much lower than those with low thermal resistances (filled-boxes curves).

Moreover, with low thermal resistances, the voltage that maximizes the COP is higher. The reason for this is that having a bad heat dissipation, the COP of the TESC system decreases for a certain voltage, as it can be seen in Figure 9, moving the optimum voltage to lower values, where the efficiency of the thermoelectric modules is not that low and can balance out the increase achieved in the cooling capacity against the extra consumption of the TEMs. This fact can cause a negative effect on the TESC with high thermal resistances and high voltages supplied to the modules, getting worse values of COP compared to the base cycle, as it has been shown in Figure 10. On the contrary, with low thermal resistances, meaningful improvements on the overall COP can be reached, for instance, a maximum increase of 20.9 % compared to de CO_2 base refrigeration cycle, and an increase of 13.3 % compared to a system that includes an IHX. The effect is more remarkable when the number of modules installed increases.

A summary of all the combinations for the thermal resistances of the heat exchangers on both sides and the number of modules is presented in Figure 11, where the values have been calculated for the optimum gas-cooler pressure and voltage supplied to the thermoelectric modules of the TESC system.

Finally, Table 4 shows a summary of the results that can be obtained from the CO_2 system using two different hot side heat exchangers at the TESC system, water cooling and heat-pipes. The former would be suitable in those applications where the gas-cooler also works with water, the latter would use heat-pipe heat exchangers and convection with air to the ambient.

Thermal resistances experimentally obtained in a previous work [42] present values of $R^t_{hhe} = 0.03\ K/W$ for the water, and $R^t_{hhe} = 0.2\ K/W$ for the air. Setting $R^t_{che} = 0.3\ K/W$ for the cold side and changing the number of modules installed between 4 and 20, the results show significant progresses, as Table 4 presents. Compared to the base cycle is possible to increase the COP in a 24 % using a water cooling system and 19.7

523 % with air; and the cooling capacity can be increased by 33.3 % and 25.6 % respectively. When comparing to
524 the cycle that includes an IHX, these improvements in the COP reach 16.3 % and 12.2 % using water and air;
525 and the increments in the cooling capacity go up to 26.9 % and 19.5 %.

526 These results present thermoelectric subcooling as an attractive technology to improve medium-small size
527 cooling capacity CO_2 refrigeration systems where mechanical subcooling is not profitable.

528

529 ## 5. CONCLUSIONS

530 This work has implemented a global computational model able to solve simultaneously a vapour compression
531 refrigeration system using CO_2 in transcritical conditions as working fluid, and a thermoelectric subcooling
532 system (TESC) installed at the outlet of the gas-cooler of the plant. Using the computational tool, a study and
533 optimization has been performed simulating the conditions of a small cooling capacity CO_2 system, varying
534 the number of modules placed (TEM), the electric voltage supplied to them, and the thermal resistances of the
535 heat exchangers employed in the TESC system. The results obtained prove the benefits of including such a
536 system in the plant analysed, getting significant improvements in both, efficiency and cooling capacity,
537 preventing the increase of the superheating degree that happens when an internal heat exchanger, IHX, is used.

538 When using 20 TEM that are being refrigerated by air, and working on optimum conditions, an increase of
539 19.7 % in the overall COP can be achieved compared to the base cycle. This increment is of 12.2 % if it is
540 compared to de IHX system. If the TEMs' cooling system is improved, this progress can be enhanced, reaching
541 an increase of 24 % in the COP and of 33.3 % in the cooling capacity.

542 Finally, this study has shown the importance of making a deep analysis of the combination of these two
543 technologies, vapour compression and thermoelectric subcooling system to optimize the working conditions,
544 related to the gas-cooler pressure and voltage supplied to the modules, which are also dependent on the ambient
545 temperature.

546 ## ACKNOWLEDGEMENTS

547 The authors would like to acknowledge the support of the Spanish Ministry of Science, Innovation and
548 Universities for the funding under the FPU Program (FPU16/05203).

549 **REFERENCES**

550 [1] Regulation (EC) No 2037/2000. Regulation (EC) No 2037/2000 of the European Parliament
551 and the Council of 29 June 2000 on substances that deplete the ozone layer. Off J Eur
552 Communities 2000;4:L244/1-24.
553 [2] The European Parliament and the Council of the European Union. REGULATION (EC) No.
554 1005/2009. Off J Eur Union 2009;L 286, 52.
555 [3] European Commission. Directive 2006/40/EC of the European Parliament and of the Council
556 of 17 May 2006 relating to emissions from air-conditioning systems in motor vehicles and
557 amending Council Directive 70/156/EEC. Off J Eur Union 2006:12–8.
558 doi:http://data.europa.eu/eli/dir/2006/40/oj.
559 [4] European Commission. Regulation (EU) No 517/2014 of the European Parliament and of the
560 Council of 16 April 2014 on fluorinated greenhouse gases and repealing Regulation (EC) No
561 842/2006. Off J Eur Union 2014;2014:L150/195-230. doi:https://doi.org/10.4271/1999-01-
562 0874.
563 [5] HAFNER A, HEMMINGSEN AK. R744 refrigeration technologies for supermarkets in warm
564 climates. 24th IIR Int. Conf. Refrig., Yokohama, Japan: 2015.
565 doi:http://dx.doi.org/10.18462/iir.icr.2015.0168.
566 [6] Kim MH, Pettersen J, Bullard CW. Fundamental process and system design issues in CO2
567 vapor compression systems. vol. 30. 2004. doi:10.1016/j.pecs.2003.09.002.
568 [7] Sanz-Kock C, Llopis R, Sánchez D, Cabello R, Torrella E. Experimental evaluation of a
569 R134a/CO2 cascade refrigeration plant. Appl Therm Eng 2014;73:39–48.
570 doi:10.1016/j.applthermaleng.2014.07.041.
571 [8] Llopis R, Sánchez D, Sanz-Kock C, Cabello R, Torrella E. Energy and environmental
572 comparison of two-stage solutions for commercial refrigeration at low temperature: Fluids and
573 systems. Appl Energy 2015;138:133–42. doi:10.1016/j.apenergy.2014.10.069.
574 [9] Catalán Gil J, Sánchez D, Doménech R, Nebot Andres L, Cabello López R. Evaluación
575 Energética de Sistemas Booster con CO2. 2017.
576 [10] Elbel S, Lawrence N. Review of recent developments in advanced ejector technology. Int J
577 Refrig 2016;62:1–18. doi:10.1016/j.ijrefrig.2015.10.031.
578 [11] Hafner A, Banasiak K, Herdlitschka T, Fredslund K, Girotto S, Haida M, et al. R744 ejector
579 system case: Italian supermarket, Spiazzo. Refrig Sci Technol 2016:511–8.
580 [12] Lawrence N, Elbel S. Experimental study on control methods for transcritical CO2 two-phase
581 ejector systems at offdesign conditions. Refrig Sci Technol 2016:511–8.
582 doi:http://dx.doi.org/10.18462/iir.gl.2016.1083.
583 [13] Lucas C, Koehler J. Experimental investigation of the COP improvement of a refrigeration
584 cycle by use of an ejector. Int J Refrig 2012;35:1595–603. doi:10.1016/j.ijrefrig.2012.05.010.
585 [14] Elbel S. Historical and present developments of ejector refrigeration systems with emphasis
586 on transcritical carbon dioxide air-conditioning. Int J Refrig 2011;34:1545–61.
587 doi:10.1016/j.ijrefrig.2010.11.011.
588 [15] Nakagawa M, Marasigan AR, Matsukawa T, Kurashina A. Experimental investigation on the
589 effect of mixing length on the performance of two-phase ejector for CO2refrigeration cycle
590 with and without heat exchanger. Int J Refrig 2011;34:1604–13.
591 doi:10.1016/j.ijrefrig.2010.07.021.
592 [16] Gullo P, Elmegaard B, Cortella G. Energy and environmental performance assessment of R744
593 booster supermarket refrigeration systems operating in warm climates. Int J Refrig
594 2016;64:61–79. doi:10.1016/j.ijrefrig.2015.12.016.
595 [17] Dai B, Liu S, Sun Z, Ma Y. Thermodynamic Performance Analysis of CO2Transcritical
596 Refrigeration Cycle Assisted with Mechanical Subcooling. Energy Procedia 2017;105:2033–
597 8. doi:10.1016/j.egypro.2017.03.579.
598 [18] Llopis R, Nebot-Andrés L, Cabello R, Sánchez D, Catalán-Gil J. Experimental evaluation of a

CO2 transcritical refrigeration plant with dedicated mechanical subcooling. Int J Refrig 2016;69:361–8. doi:10.1016/j.ijrefrig.2016.06.009.
[19] Rowe DM. Thermoelectrics Handbook: Macro to Nano. 1st ed. Boca Raton: 2006.
[20] Hermes CJL, Barbosa JR. Thermodynamic comparison of Peltier, Stirling, and vapor compression portable coolers. Appl Energy 2012;91:51–8. doi:10.1016/j.apenergy.2011.08.043.
[21] Zhao D, Tan G. A review of thermoelectric cooling: Materials, modeling and applications. Appl Therm Eng 2014;66:15–24. doi:10.1016/j.applthermaleng.2014.01.074.
[22] Chein R, Huang G. Thermoelectric cooler application in electronic cooling. Appl Therm Eng 2004;24:2207–17. doi:10.1016/j.applthermaleng.2004.03.001.
[23] Cai Y, Liu D, Zhao FY, Tang JF. Performance analysis and assessment of thermoelectric micro cooler for electronic devices. Energy Convers Manag 2016. doi:10.1016/j.enconman.2016.07.011.
[24] Gong T, Gao L, Wu Y, Zhang L, Yin S, Li J, et al. Numerical simulation on a compact thermoelectric cooler for the optimized design. Appl Therm Eng 2019;146:815–25. doi:10.1016/J.APPLTHERMALENG.2018.10.047.
[25] Min G, Rowe DM. Experimental evaluation of prototype thermoelectric domestic-refrigerators. Appl Energy 2006;83:133–52. doi:10.1016/j.apenergy.2005.01.002.
[26] Lee JS, Rhi SH, Kim CN, Lee Y. Use of two-phase loop thermosyphons for thermoelectric refrigeration: Experiment and analysis. Appl Therm Eng 2003;23:1167–76. doi:10.1016/S1359-4311(03)00043-7.
[27] Vián JG, Astrain D. Development of a thermoelectric refrigerator with two-phase thermosyphons and capillary lift. Appl Therm Eng 2009;29:1935–40. doi:10.1016/j.applthermaleng.2008.09.018.
[28] Omer SA, Riffat SB, Ma X. Experimental investigation of a thermoelectric refrigeration system employing a phase change material integrated with thermal diode (thermosyphons). Appl Therm Eng 2001;21:1265–71. doi:10.1016/S1359-4311(01)00010-2.
[29] Bansal PK, Martin A. Comparative study of vapour compression, thermoelectric and absorption refrigerators. Int J Energy Res 2000;24:93–107. doi:10.1002/(SICI)1099-114X(200002)24:2<93::AID-ER563>3.0.CO;2-6.
[30] Çağlar A. Design and experimental investigation of a novel thermoelectric water dispenser unit. Appl Therm Eng 2019;149:822–8. doi:10.1016/J.APPLTHERMALENG.2018.11.028.
[31] Al-Madhhachi H, Min G. Effective use of thermal energy at both hot and cold side of thermoelectric module for developing efficient thermoelectric water distillation system. Energy Convers Manag 2017;133:14–9. doi:10.1016/J.ENCONMAN.2016.11.055.
[32] Gao Y-W, Meng J-H, Liu H-B, Chen W-H, Wang X-D. Transient supercooling behaviors of a novel two-stage Peltier cooler. Appl Therm Eng 2018;143:248–56. doi:10.1016/J.APPLTHERMALENG.2018.07.100.
[33] Lv H, Wang X-D, Meng J-H, Wang T-H, Yan W-M. Enhancement of maximum temperature drop across thermoelectric cooler through two-stage design and transient supercooling effect. Appl Energy 2016;175:285–92. doi:10.1016/J.APENERGY.2016.05.035.
[34] Vián JG, Astrain D. Development of a hybrid refrigerator combining thermoelectric and vapor compression technologies. Appl Therm Eng 2009;29:3319–27. doi:10.1016/j.applthermaleng.2009.05.006.
[35] Astrain D, Martínez A, Rodríguez A. Improvement of a thermoelectric and vapour compression hybrid refrigerator. Appl Therm Eng 2012;39. doi:10.1016/j.applthermaleng.2012.01.054.
[36] Enescu D, Virjoghe EO. A review on thermoelectric cooling parameters and performance. Renew Sustain Energy Rev 2014;38. doi:10.1016/j.rser.2014.07.045.
[37] Sánchez D, Cabello R, Llopis R, Torrella E. Development and validation of a finite element model for water – CO2 coaxial gas-coolers. Appl Energy 2012;93:637–47. doi:10.1016/J.APENERGY.2011.12.100.

[38] Aprea C, Maiorino A. An experimental evaluation of the transcritical CO2refrigerator performances using an internal heat exchanger. Int J Refrig 2008;31:1006–11. doi:10.1016/j.ijrefrig.2007.12.016.
[39] Torrella E, Sánchez D, Llopis R, Cabello R. Energetic evaluation of an internal heat exchanger in a CO2transcritical refrigeration plant using experimental data. Int J Refrig 2011;34:40–9. doi:10.1016/j.ijrefrig.2010.07.006.
[40] Marlow Industries Inc. Marlow TG12-8 Datasheet 2016:1–2.
[41] Araiz M, Catalán L, Herrero O, Rodriguez A, Pérez MG. The Importance of the Assembly in Thermoelectric Generators. Bringing Thermoelectr into Real 2018.
[42] Astrain D, Aranguren P, Martínez A, Rodríguez A, Pérez MG. A comparative study of different heat exchange systems in a thermoelectric refrigerator and their influence on the efficiency. Appl Therm Eng 2016;103:1289–98. doi:10.1016/j.applthermaleng.2016.04.132.

FIGURES

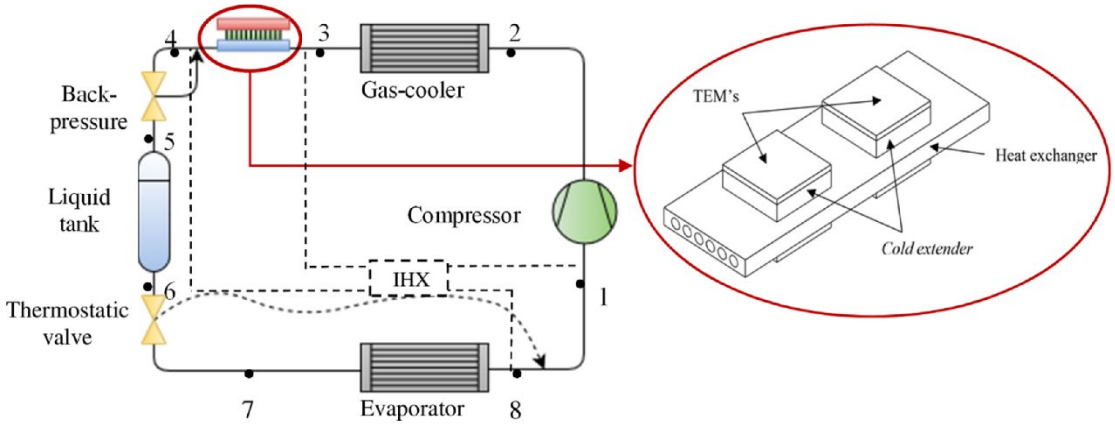

Figure 1. CO2 refrigeration system schematic diagram.

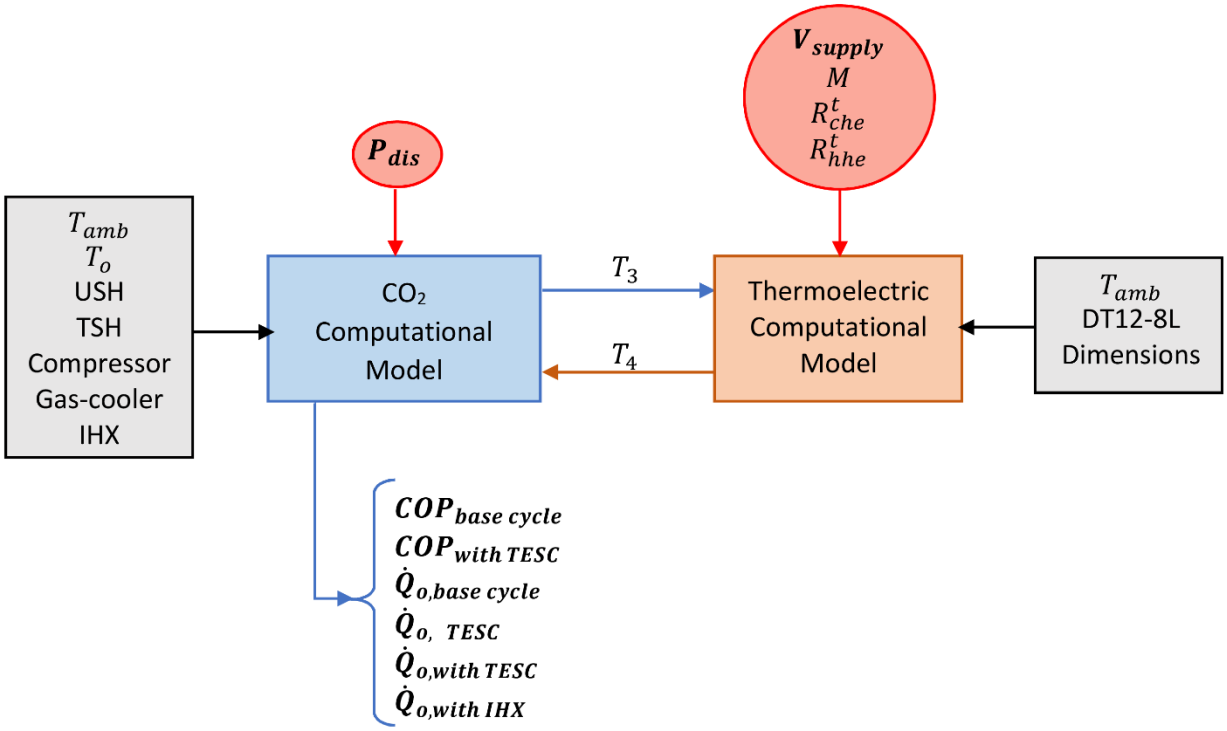

680

681 **Figure 2.** Calculation methodology diagram

682

683

684

685

686

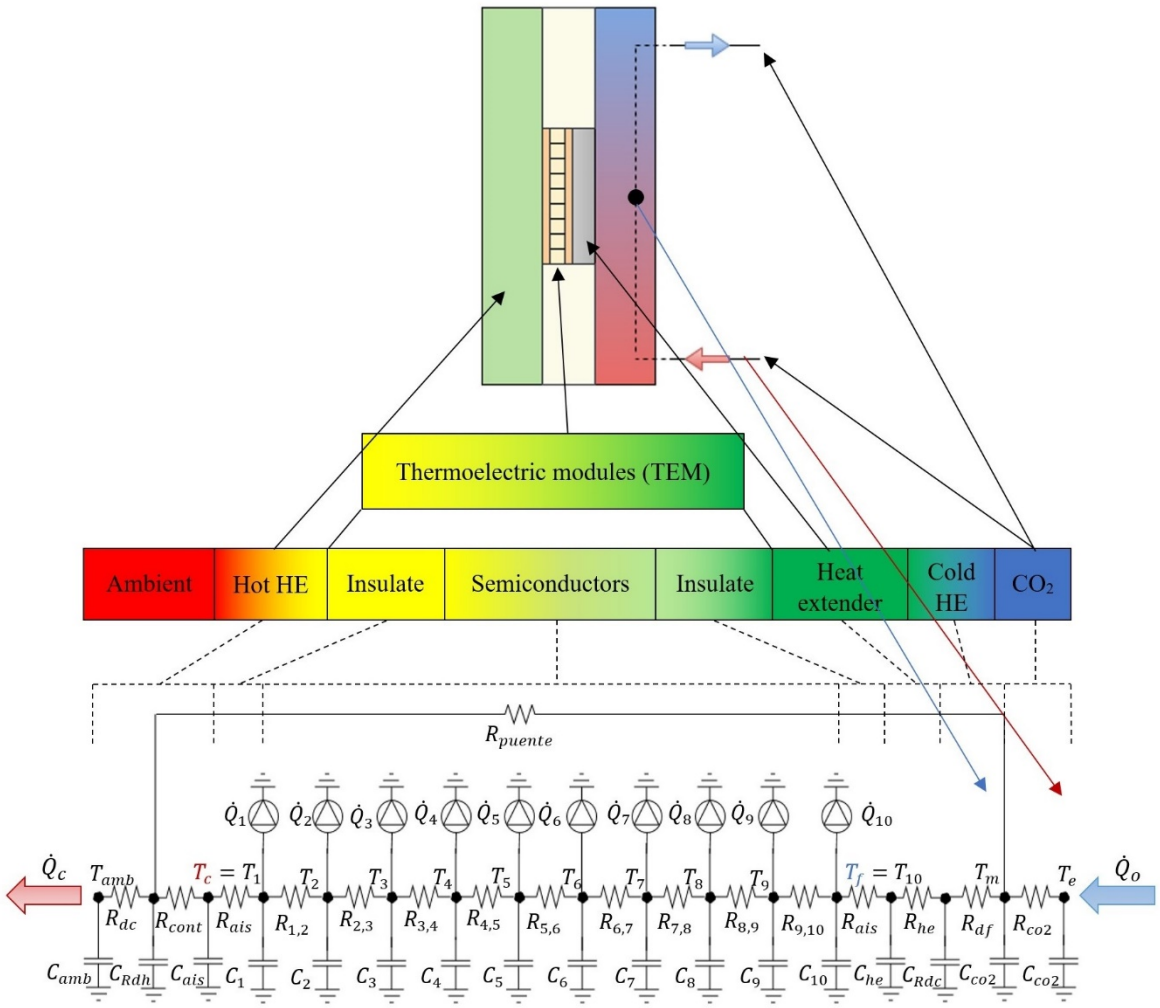

687

688 **Figure 3**. Discretization of the TESC system to be solved by the computational model.

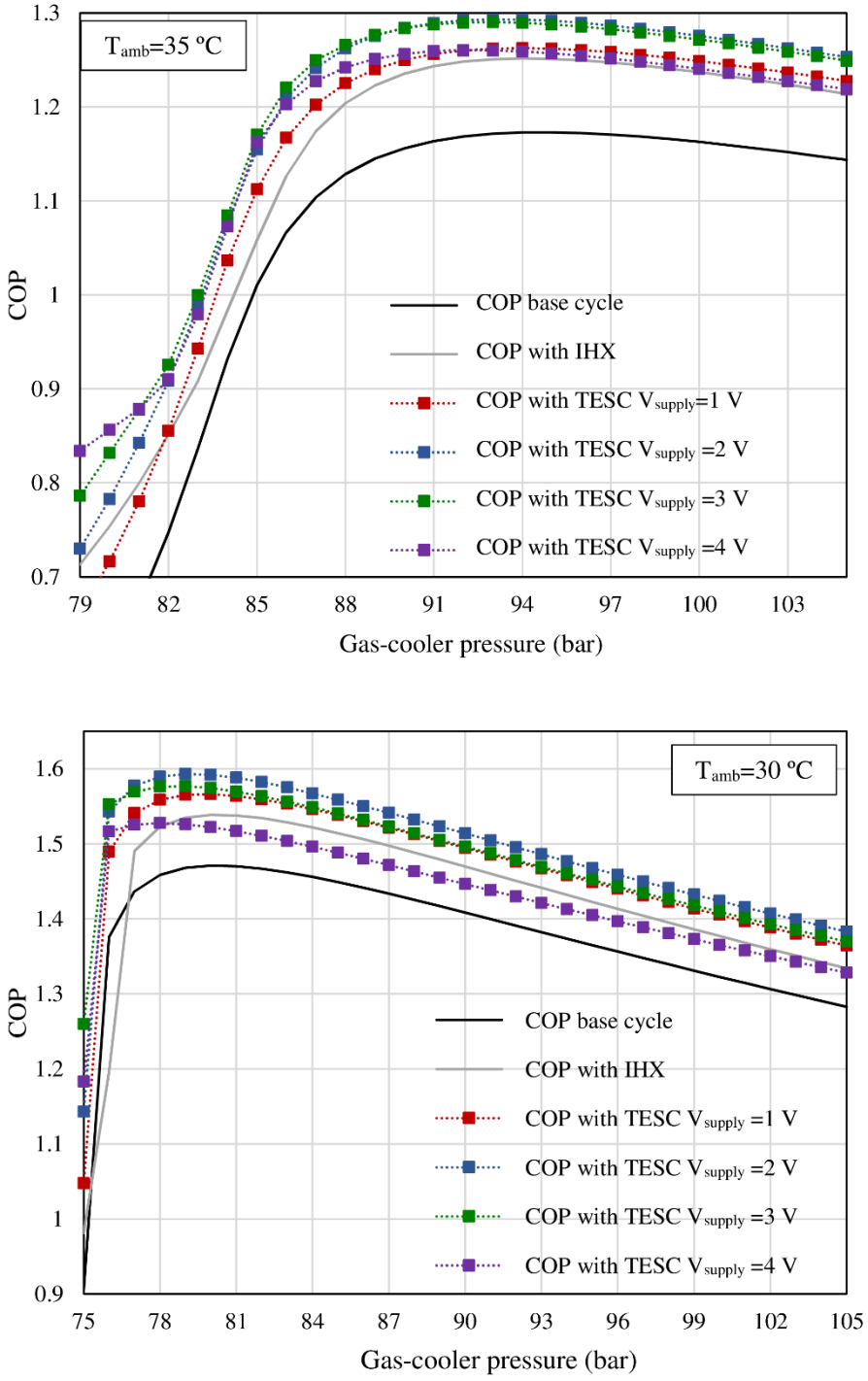

689

690 **Figure 4**. Overall COP of the plant as a function of the gas-cooler pressure and the voltage supplied
691 to the TEMs.

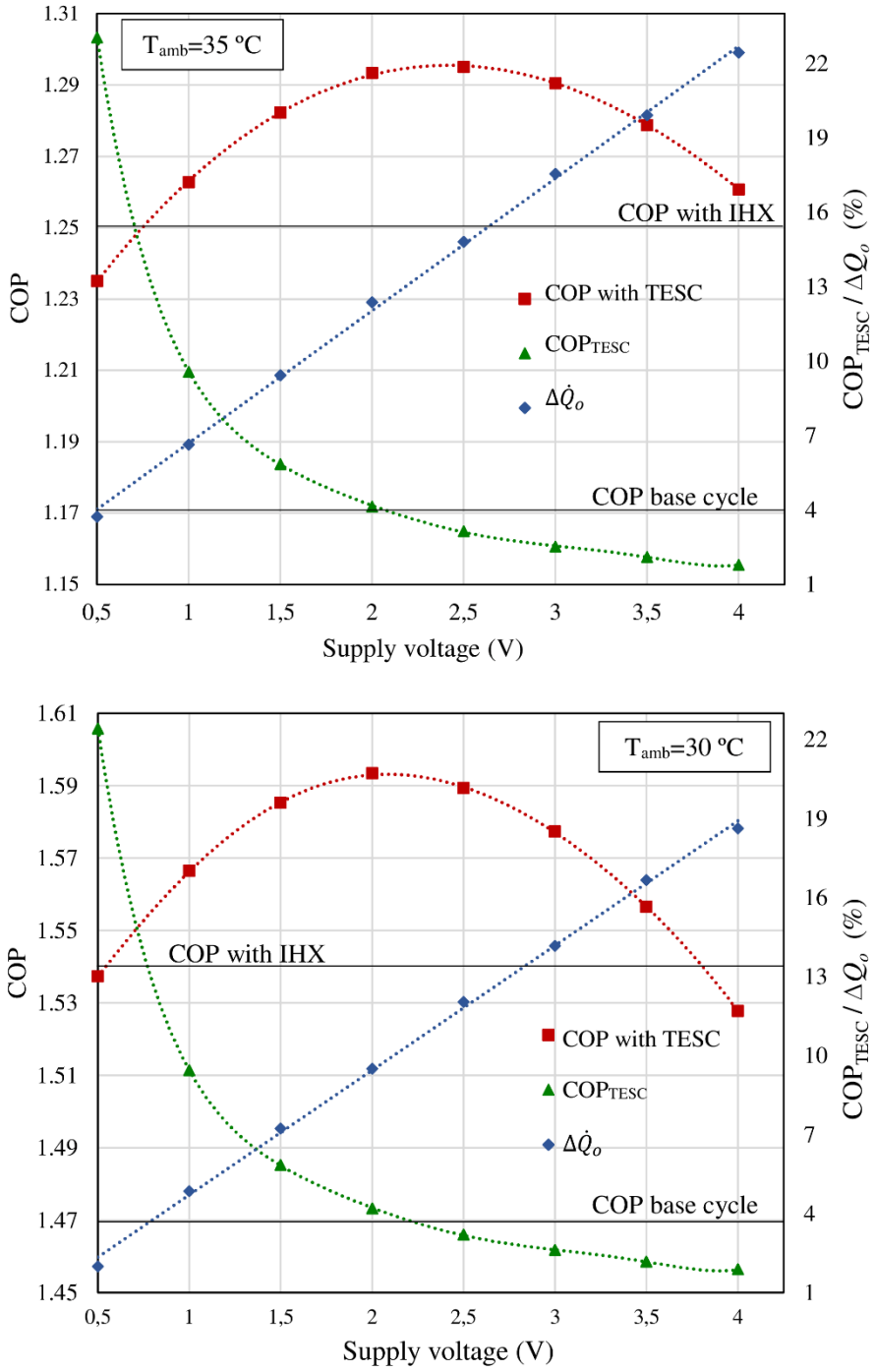

692

693 **Figure 5.** COP of the TEMs, overall COP and increment of the cooling capacity vs the voltage
694 supplied to the modules, considering an ambient temperature of 35 °C and 30 °C respectively.

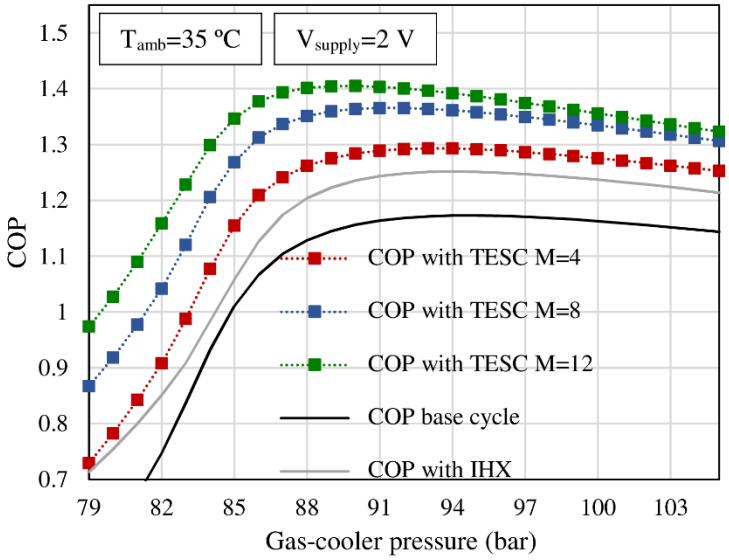

695

696 **Figure 6.** Overall COP variation as a function of the gas-cooler pressure and the number of TEMs
697 installed, considering a voltage of 2 V, an ambient temperature of 35 °C and an evaporation
698 temperature of -10 ºC.

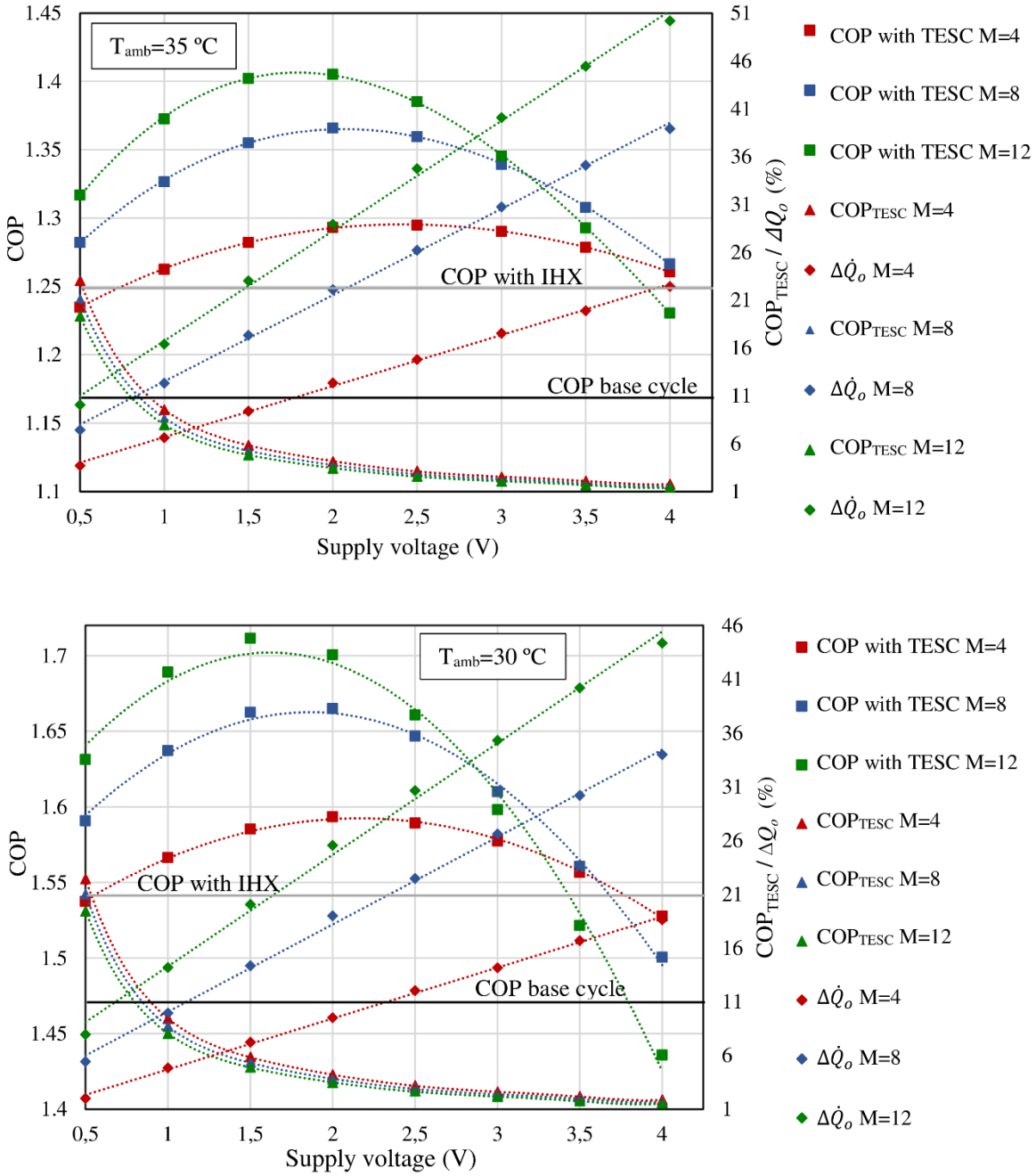

Figure 7. Thermoelectric modules COP, overall COP and increment of the cooling capacity vd the operating voltage supplied to the TEMs for different number of modules installed, considering 35°C and 30°C as ambient temperature and an evaporation temperature of -10 ºC.

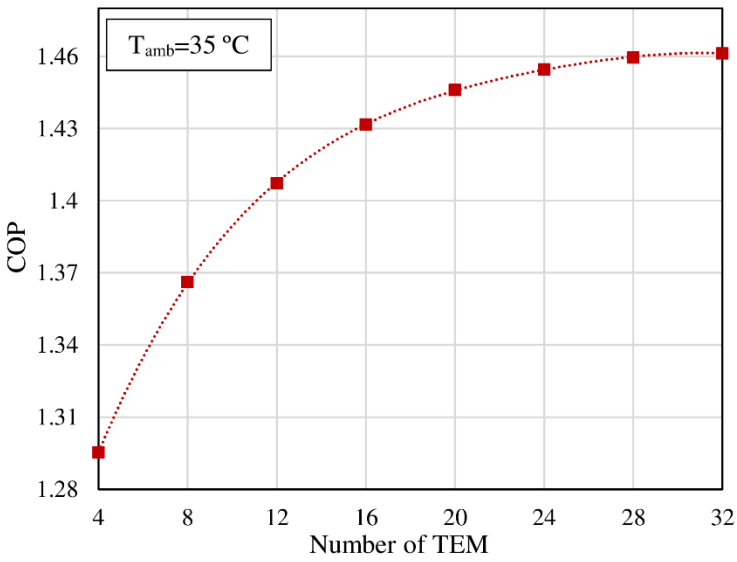

Figure 8. Overall optimum COP as a function of the number of modules installed, for an ambient temperature of 35 ° C and an evaporation temperature of -10 ºC.

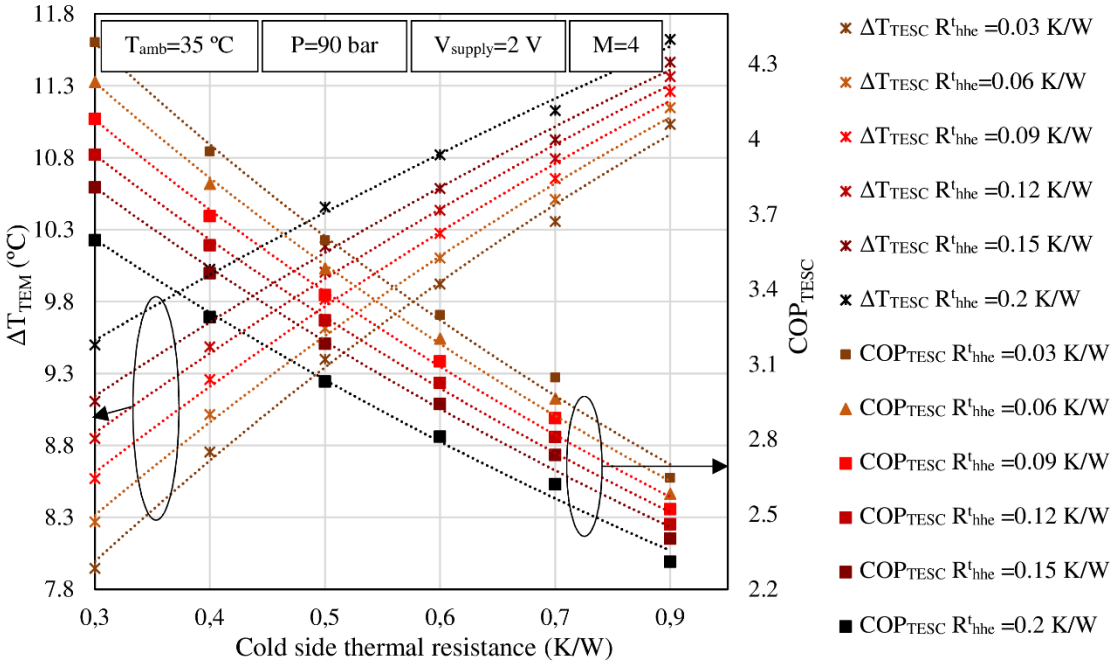

Figure 9. ΔT_{TEM} y COP_{TESC} as a funtion of the thermal resistance per module of the cold side heat for several thermal resistances of the hot side. T_{amb}=35 ºC, V_{supply}=2 V, P=90 bar and n=4.

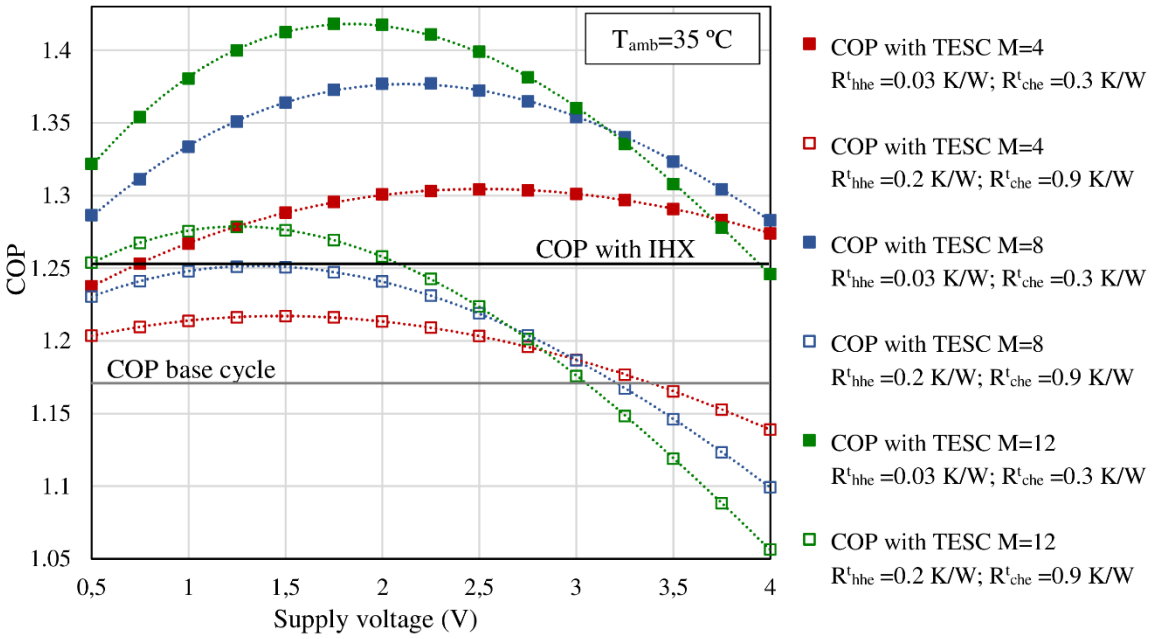

Figure 10. Overall COP of the system vs voltage supplied to the TEM for several thermal resistances and number of modules. T_{amb} = 35 °C.

Number of TEM	COP increment compared to the base cycle	COP increment compared to the base cycle with IHX
4	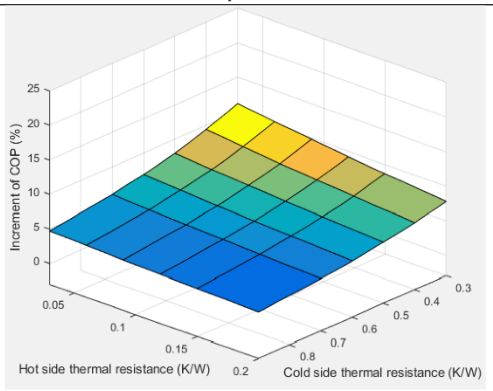	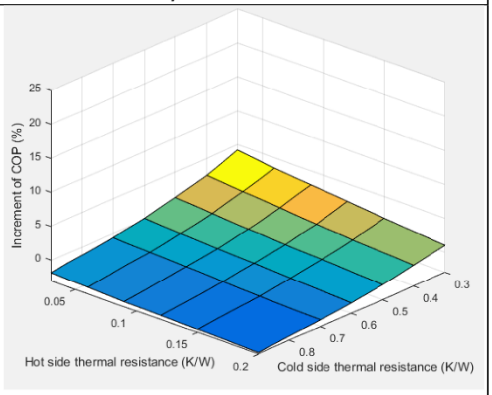
12	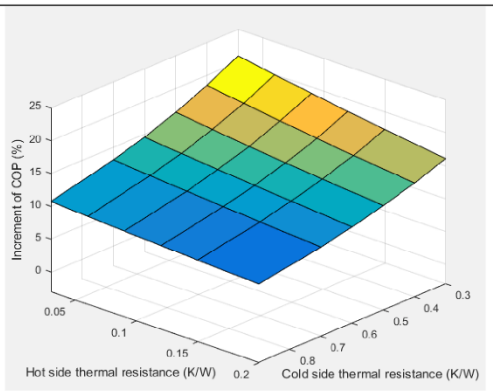	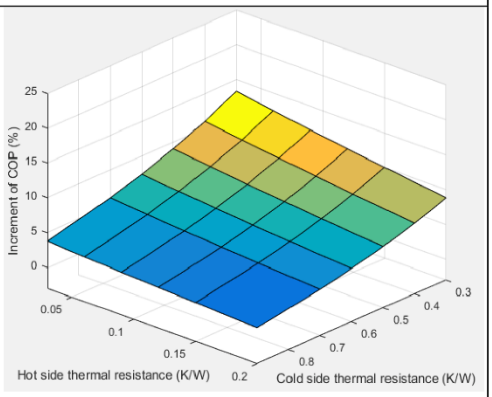
20	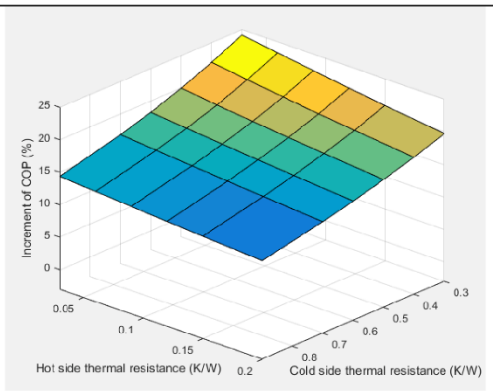	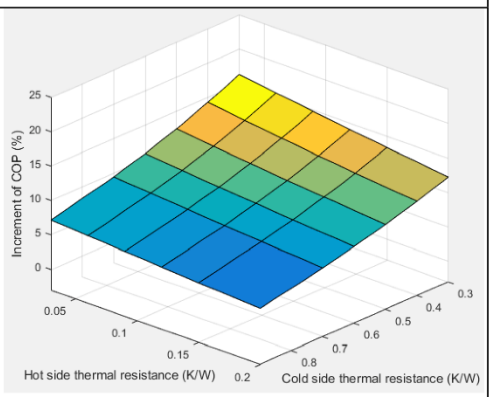

718

719 **Figure 11.** Overall COP increments when including a TESC system as a function of the thermal
720 resistances of the heat exchangers and the number of thermoelectric modules. T_{amb} = 35 °C.

721

722

TABLES

Table 1. Experimental expression for the efficiencies of the compressor.

Volumetric efficiency	Global efficiency
$\eta_V = a_0 + a_1 \cdot P_{ev} + a_2 \cdot P_{gc} + a_3 \cdot T_{comp,\ in}$	$\eta_G = b_0 + b_1 \cdot P_{ev} + b_2 \cdot P_{gc} + b_3 \cdot T_{comp,\ in}$
a_0: 0.874861446085	b_0: 0.522830324579
a_1: 0.004671565378	b_1: -0.000163701663
a_2: -0.003566505990	b_2: -0.000212045252
a_3: 0.002209861792	b_3: 0.001704083987
e_{max}: 6.5% σ: 0.01	e_{max}: 7.3% σ: 0.01
P_{ev} = [26.3 ÷ 35.3] bar P_{gc} = [60.2 ÷ 100.3] bar $T_{comp,\ in}$ = [-2.5 ÷ 19.9] ºC	

Table 2. Thermoelectric parameters considered at the computational model

Parameter	Value	Units	Description
N	127		Number of thermoelectric pairs
L_{tp}	1.3	mm	Length of the thermoelectric pair
A_{tp}	1.4 x 1.4	mm^2	Cross sectional area of the thermoelectric pair
cp_{tp}	544.28	J/kgK	Specific heat of the thermoelectric pair
d_{tp}	6892	Kg/m^3	Density of the thermoelectric pair
L_{cer}	0.75	mm	Length of the ceramic
A_{cer}	40 x 40	mm^2	Cross sectional area of the ceramic
k_{cer}	35	W/mK	Thermal conductivity of the ceramic layer
d_{cer}	3900	Kg/m^3	Density of the ceramic
cp_{cer}	850	J/kgK	Specific heat of the ceramic
L_u	0.45	mm	Length of the union
A_u	4.2 x 1.85	mm^2	Cross sectional area of the union
cp_u	385	J/kgK	Specific heat of the union
d_u	8930	Kg/m^3	Density of the union
ρ_u^{sup}	0.000011	Ωcm^2	Superficial electrical resistivity of the union material

734 **Table 3.** Results of the simulations for optimum gas-cooler pressure and optimum voltage supplied
735 to the TEMs.
736

Ambient temperature (°C)	**25**	**30**	**35**
Optimum discharge pressure (bar)	75	79	93
Optimum operating voltage (V)	1.5	2	2.5
COP $_{\text{base cycle}}$	1.82	1.47	1.17
COP $_{\text{with IHX}}$	1.87	1.54	1.25
COP $_{\text{with TESC}}$	1.92	1.59	1.30
ΔCOP $_{\text{base cycle - with TESC}}$ **(%)**	5.40	8.32	10.40
ΔCOP $_{\text{with IHX - with TESC}}$ **(%)**	2.44	3.55	3.48
$\dot{Q}_o$ $_{\text{base cycle}}$ **(W)**	198.49	166.21	146.01
$\dot{Q}_o$ $_{\text{with IHX}}$ **(W)**	201.98	174.21	154.79
$\dot{Q}_o$ $_{\text{with TESC}}$ **(W)**	215.18	189.08	172.17
$\Delta\dot{Q}_o$ $_{\text{base cycle - with TESC}}$ **(%)**	8.41	12.56	16.86
$\Delta\dot{Q}_o$ $_{\text{with IHX - with TESC}}$ **(%)**	6.54	8.54	11.23

737

738 **Table 4.** Results for the TESC system using water or air cooling system for 4, 12 and 20 TEMs.
739

COP $_{\text{max}}$	**COP** $_{\text{TESC}}$	**P** $_{\text{opt}}$ **(bar)**	**V** $_{\text{opt}}$ **(V)**	**ΔCOP** $_{\text{base cycle - with TESC}}$ **(%)**	**ΔCOP** $_{\text{with IHX - with TESC}}$ **(%)**	$\dot{Q}_o$ $_{\text{with TESC}}$ **(W)**	$\Delta\dot{Q}_o$ $_{\text{base cycle - with TESC}}$ **(%)**	$\Delta\dot{Q}_o$ $_{\text{with IHX - with TESC}}$ **(%)**	**M**
WATER COOLING $(R^t_{hhe} = 0.03\ K/W)$									
1.30	3.27	93	2.5	11.20	4.22	173.55	17.80	12.12	4
1.42	4.17	89.5	1.75	20.91	13.33	190.19	29.09	22.87	12
1.46	4.34	87.5	1.5	24.12	16.34	196.35	33.27	26.85	20
AIR COOLING $(R^t_{hhe} = 0.2\ K/W)$									
1.26	3.53	94	2	7.79	1.03	164.81	11.87	6.47	4
1.36	3.51	91	1.75	16.07	8.79	183.30	24.41	18.41	12
1.40	4.67	89.5	1.25	19.75	12.24	185.03	25.56	19.53	20

740

741

742